PS-PVD Processing of Single-Phase Lanthanum Tungstate Layers for Hydrogen-Related Applications

D. Marcano[1], M. E. Ivanova[1], G. Mauer[1*], Y. J. Sohn[1], A. Schwedt[2], M. Bram[1], N. H. Menzler[1], R. Vaßen[1]

[1]Forschungszentrum Jülich GmbH, Institute of Energy and Climate Research: IEK-1 Jülich - Germany

[2]Gemeinschaftslabor für Elektronenmikroskopie RWTH Aachen – Germany

* Corresponding author, E-mail: g.mauer@fz-juelich.de

Abstract

This work presents a systematic study of the lanthanum tungstate (LaWO) ceramic layers formation on porous metallic substrates as a function of the PS-PVD processing parameters including plasma characteristics, support type and temperature, as well as addition of O_2 during the spraying. Through precise control of the PS-PVD parameters, a set of processing conditions were found that led to He gas-tight purely cubic LaWO layers with negligible secondary phase precipitations. Being dependent on process conditioning, the formation and evolution of the cubic $La_{6-x}WO_{12-\delta}$ (x = 0.3-0.6) as the main phase of functional importance and of the undesired secondary phases (La_2O_3 and $La_6W_2O_{15}$) was strongly affected by the cation and oxygen stoichiometries. The rapid cooling of the feedstock at particle impact on the substrate led to the formation of highly La-saturated compositions which exhibited significant lattice expansion in comparison with conventionally processed LaWO and is considered beneficial in terms of material performance. And indeed, the H_2 permeation performance of the PS-PVD processed LaWO ceramic layers shown earlier by our group was 0.4 ml/min·cm^2 at 825°C for 60 µm thickness of the functional layer, the highest value reported for this type of proton conducting ceramics, so far.

Keywords

Lanthanum tungstate, Proton conducting ceramics, Functional ceramic coatings, H_2 separation, Crofer®22APU supported ceramic coatings, Plasma Spray-Physical Vapor Deposition (PS-PVD), Electron Backscatter Diffraction (EBSD).

1. Introduction

Lanthanum tungstate ($La_{6-x}WO_{12-\delta}$, with x = 0.3-0.6, further referred to as LaWO) is a promising ceramic material for H_2-related applications. The cubic polycrystalline LaWO phase is a predominant proton conductor at temperatures below 700°C in humid atmospheres and a mixed proton-electronic conductor above this temperature in reducing atmospheres [1-3]. Such properties, accompanied with significant thermo-chemical stability in a variety of gas conditions (including CO, CO_2, H_2, steam) [4-6], make it a promising candidate for applications at lower as well as at elevated temperatures. Target applications are as a solid electrolyte for proton conducting solid oxide cells (PC-SOCs) [7-9], as ceramic membranes for H_2 separation from gas mixtures, in catalytic membrane reactors for CO_2 utilization (e.g. CO_2/H_2O co-electrolysis to biofuels and other valuable chemicals), and in water gas shift process (WGS, $CO+H_2O \leftrightarrow CO_2+H_2$) with simultaneous H_2 extraction [7,8,10].

Lanthanum tungstates are compounds within the La_2O_3-WO_3 solid solution system and are usually formed at temperatures above 1100°C. At these temperatures, the single-phase domain broadens and shifts toward higher La/W ratios as shown in our previous works [4,11] and that of Magraso et al. [12]. This reflects the incorporation of more La_2O_3 at a given stoichiometry, which leads to better conductivity properties [1,12]. At 1400°C-1500°C, the single cubic phase domain is limited within the La/W ratios of 5.3-5.7 [4,11,12]. Beyond this range, hexagonal La_2O_3 (high La/W) and orthorhombic $La_6W_2O_{15}$ (low La/W) secondary phases are segregated. These two phases are also formed as decomposition products of the cubic $La_{10}W_2O_{21}$ phase which is only stable below 1100°C (in vacuum) [13]. Their presence in large amounts, along with the main proton conducting cubic LaWO phase, leads to

detrimental degradation of the mechanical and conductivity performance [4,14]. Hence, in every approach to fabricate components based on LaWO, the identification of optimal processing conditions to form single cubic LaWO phase is of great importance.

In this work, plasma spray-physical vapor deposition (PS-PVD) is employed to manufacture dense coatings of single cubic phase LaWO deposited on graphite and on porous ferritic stainless steel. Graphite supports were applied mostly to study the effect of processing parameters on the chemical and phase compositions of the coatings. These types of supports could be easily removed and the free-standing coatings analyzed, which is not the case for the steel supports (details in section 2.5).

Compared to other processing routes, PS-PVD is a technique which allows for lower deposition temperatures (800-1000°C) in much shorter times than conventionally applied. Classical routes for processing of LaWO ceramics usually require sintering temperatures in the range of 1450-1550°C for up to 12 h [1,12]. Such conditions might lead to stoichiometric deviations due to WO_3 evaporation and pronounced secondary phase segregations (e.g., La_2O_3). Lower fabrication temperatures as in the case of PS-PVD will restrict such effects allowing for optimal coating composition without subsequent sintering being necessary. Due to the lower processing temperature, it is also possible to apply steel substrates. On the other hand, during the spray process, the feedstock will see much higher temperatures than typical sintering temperatures, however only for short periods of time. Also, the local temperature during deposition might be considerably higher than the mean deposition temperature. Hence, it has to be evaluated if these short temperature excursions are detrimental for the development of suitable phases.

PS-PVD takes place under reducing conditions and very rapid cooling rates. These features allow controlling the phase formation by adjusting the oxygen partial pressure in the process chamber and inhibiting diffusion processes which might advance secondary phases segregations. Previous works of our group demonstrated the employment of the PS-PVD method for manufacturing of oxygen permeable membranes based on lanthanum strontium

cobalt iron oxides (LSCF), as well as of yttria stabilized zirconia (YSZ) electrolytes for solid oxide fuel cells (SOFCs) on porous metallic supports [15-17]. In these works, the resulting LSCF and YSZ functional layers were proven to be He gas-tight (a value of $1 \cdot 10^{-4}$ mbar·l/s·cm^2 was set as a post-fabrication He leakage threshold) and stable with outstanding performances as reflected by the O_2 permeation flux and the open cell voltage (OCV) values, respectively.

In conventional processing, as for example by tape casting, the functional layer is deposited on a ceramic or metallic substrate. During co-sintering, densification of this layer is significantly promoted by the faster shrinkage of the porous support. In the advanced sintering stage, when the ceramic coating has achieved a high degree of densification and becomes quite rigid, it significantly constrains the further shrinkage of the porous substrate. Therefore, the co-sintering of structures with significantly mismatching sintering properties usually leads to geometric deformation and bending of the overall assembly, thus being problematic from the application point of view. Hence, significant efforts were made to understand these effects in LaWO-based ceramic systems [18,19]. Another issue of the co-firing is that in the case of a metallic supports made by tape casting (as used in the present work), these can only be sintered in non-oxidizing atmosphere at a maximum of 1100°C, while the LaWO ceramics require significantly higher temperatures to densify. In this context, the PS-PVD technique is considered as an advantageous approach for the formation of single-phase LaWO ceramic layers on metallic substrates. As pointed out, further sintering is neither required for achieving functional layer densification, nor for organic components release (binders/solvents) used in the wet chemical processing. Using metallic supports for functional ceramic coatings allows for integration into a module or chemical reactor by means of welding, for example, and ensures high mechanical stability of the assembly during processing and sealing. In terms of achieving thermo-mechanical compatibility between the ceramic coating and the metallic substrate, materials with matching coefficients of thermal expansion (CTE) usually need to be combined. Any residual stresses origin mainly from the deposition process and/or precipitation formation.

The aim of this study is to carry out a systematic research for understanding the influence of PS-PVD processing parameters on the formation of single cubic LaWO phase on metallic porous substrates. The reducing atmospheres and very fast cooling rates are exploited to control the oxygen stoichiometry and formation of precipitates. In a previous work [13] it has been shown that under vacuum of 10^{-4} Pa it is possible to have the coexistence of both $La_2O_3/La_6W_2O_{15}$ secondary phases at a cationic stoichiometry where only $La_{10}W_2O_{21}$ would exist at standard pressure conditions. Obviously, the oxygen partial pressure is the controlling factor. Hence, it is of interest to validate the phase formation under PS-PVD low-pressure conditions (typical chamber pressure 100-300 Pa which is six orders of magnitude higher than the mentioned vacuum conditions) and in addition to vary the oxygen stoichiometry among other control parameters.

2. Experimental

2.1. Manufacturing of porous metallic supports

In this work, porous metallic supports were made of Crofer22®APU (later referred to as Crofer) using a processing route developed in-house [20]. Material designations are 1.4760 according to DIN and EN standards as well as UNS S 4535 according to ASTM. This high-temperature ferritic stainless steel was especially developed for application in solid oxide fuel cells (SOFCs). It was chosen as a support material in this work since its coefficient of thermal expansion (CTE_{Crofer}=12.3x10^{-6} K^{-1}, 800-1000°C) is similar to that of LaWO (CTE_{LaWO} =11-12x10^{-6} K^{-1}). Substrates were manufactured in-house by tape casting a slurry made of atomized ferritic steel Crofer powder provided by H.C. Starck, Germany. The powder fraction with particle sizes below 22 µm (d_{50} = 13.3 µm) was used to prepare the alcohol based slurry. Apart from ethanol used as solvent, a combination of binding (Mowital® (Polyvinylbutyral), Kuraray, Japan) and plasticizing agents was also added. The viscosity of the slurry was 20±2 Pa·s at a shear rate of 1.8 s^{-1} and solid content of 88 wt.%. The tape casting was performed on an automated tape casting device (FGA500-SAMA, Germany). By adjusting the position of the doctor blade, a green tape thickness of about 1150-1200 µm was

achieved. Substrate samples of 70x70 mm^2 were punched out of the green tape and pre-sintered at 900°C for 1 h in Ar (heating rate 5 K/min) including a de-binding step at 600°C for 30 min (heating rate of 2 K/min in the range RT-600°C). The final sintering took place at 1100°C for 2 h in Ar (heating rate 5 K/min). The dimensions of the sintered substrate samples were 15 mm in diameter (by laser cutting) and 0.9-1.0 mm in thickness with an average porosity of approximately 30% as determined by micrographs image analysis.

2.2. LaWO powder feedstock

The feedstock material for the PS-PVD processing was $La_{5.5}WO_{12-\delta}$ powder provided by Oerlikon Metco, Wohlen, Switzerland. It has an almost spherical morphology with some cavities, see Figure 1, with particle size distribution d_{10} = 8 µm, d_{50} = 13 µm, d_{90} = 19 µm determined by laser diffraction. The powder consisted of single cubic LaWO phase (determined by XRD analysis, not shown). Prior to spraying, the powder was dried in air at 80°C for 24 h to avoid agglomeration disfavoring its flowability.

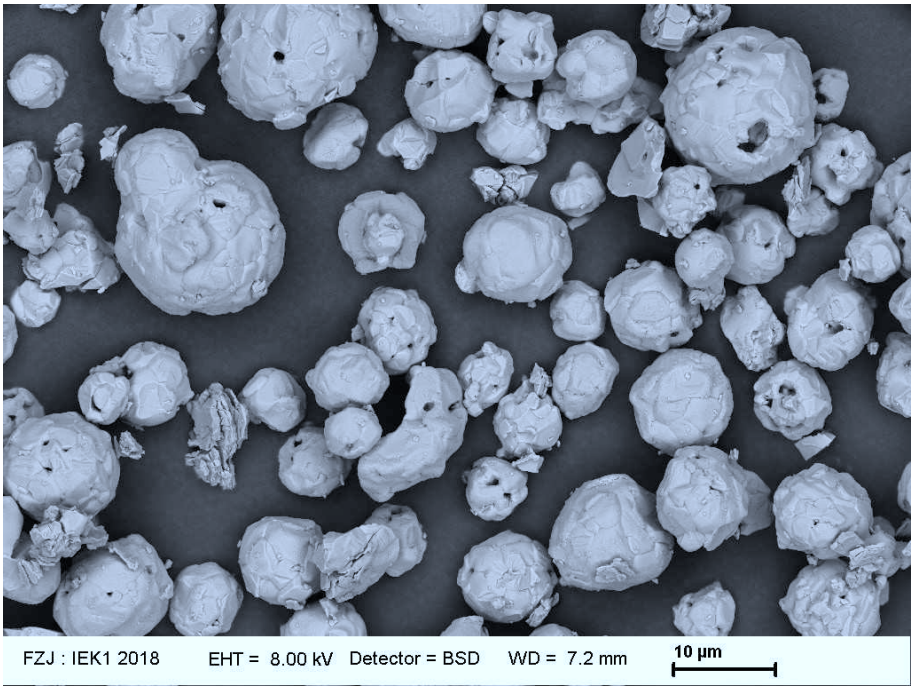

Figure 1. LaWO feedstock powder (SEM back scattered electron image).

2.3. Parameters for PS-PVD deposition of LaWO coating

The coatings were deposited by a Multicoat PS-PVD system (Oerlikon Metco, Wohlen, Switzerland) with an O3CP torch with plasma spray parameters reported in our previous works [15,17]. The feedstock powder is injected radially into the plasma jet by a carrier gas flow (Ar) through a nozzle which is located close to the plasma jet exit of the torch. The powder feed rate was 17 g/min. A current of 2000 A yielding a torch input power of 87 and 88 kW (depending on the plasma gas composition) at a chamber pressure of 250 Pa was used. The average substrate temperature was measured using a pyrometer. In order to study the effect of spray conditions on the cation content and oxygen stoichiometry in the final layer, plasma gas composition, spraying distance and addition of oxygen in the vacuum chamber during the spraying were selected as variable parameters. Phase stability of the functional layers was proved by means of post-spray annealing experiments and XRD analyses. A summary of the applied processing parameters is presented in Table 1.

Table 1. Fabrication parameters applied in the present study.

Coating	Processing parameters						
	Plasma gas flux, slpm*	Input/net power, kW	Spray distance,	Support	Average substrate temper.,	Addition O_2 slpm	Post PS-PVD annealing
A/1	Ar 100	88/	1000	Graphite	807±8	-	No
A/2	He 30	48				4	
B/1	Ar 100	88/	900	Graphite	851±15	-	No
B/2	He 30	48				4	
C/1	Ar 110 He 20	87/ 46	900	Graphite	834±4	-	No
C/2				Crofer	840±20		
C/3				Crofer			HT-XRD 10^5 Pa air
C/4				Crofer		4	HT-XRD 10^5 Pa air
C/5				Crofer			No
C/6				Crofer			10^{-2} Pa Ar
C/7				Crofer			10^5 Pa air

*slpm: standard liters per minute

To compare the three different plasma parameters A/B and C, the mass-specific net enthalpies in the plasma gas were calculated based on the plasma net power and the mass flow of the plasma gas species, see Table 2. The plasma net power was determined on the basis of the torch cooling water flow and temperature rise. They are lower for the parameter C mainly due to the higher Ar fraction. Moreover, a one-dimensional calculation of the plasma flow from the torch nozzle exit to the expanded state at the chamber pressure of 250 Pa was done. While the velocities were comparable for A/B and C (not shown), the temperatures were found to be lower for parameter C (Table 2). Assuming local thermal equilibrium (LTE) in the plasma, chemical equilibria were determined based on the

minimization of the Gibbs energy by also taking into account the ionized species [21]. For these compositions, the thermal conductivities were calculated, being an important parameter for the heat transfer from the plasma to the feedstock. They were found to be lower for parameter C as well. Thus, it can be concluded that at parameter A, the longest thermal treatment of the particles takes place due to the longer spray distance. At parameter B, the thermal treatment is shorter but more effective compared to parameter C where it is least.

Table 2. Plasma characteristics for the deposition of coatings A, B and C, see Table 1.

Parameter	**A and B**	**C**
Mass specific net enthalpy, 10^6 J/kg	15.6	13.9
Plasma temperatures at nozzle exit / in expanded jet, K	11,530 / 3400	11,440 / 3260
Thermal conductivities of the plasma at nozzle exit / in expanded jet, W/(m K)	3.41 / 0.17	3.19 / 0.14

Coating times of 3 min were chosen for all samples. In this way, layers with thicknesses of 40 to 60 µm were obtained. The Crofer substrates were described above. For these samples, a sample holder with a metallic mask was applied to keep the sample in position without constraints during the heating and cooling steps. The holder was heat conductive (however not actively cooled) since the samples were laid in a steel cavity. Thus, a stable heat flow through the sample was established. The graphite substrates were blocks of 25x25x20 mm³. In contrast to Crofer, these samples were held only by two small claws.

In addition, the influence of oxygen on the secondary phase formation was studied. 4 slpm of O_2 was added to the process chamber atmosphere during spraying. Adding more than this did not lead to considerable differences regarding the phase formation (according to our preliminary tests). After spraying, selected coatings were annealed at 900°C for 3 h in Ar and air to investigate the phase stability.

2.4. Plasma characterization

Optical emission spectroscopy (OES) measurements of the plasma jet were conducted. Wavelengths in the range of 381-786 nm were scanned, and the radiation was collected with a set of achromatic lenses, transferred by an optical fiber and detected by a 1024x1024 CCD array. The spectrometer (ARYELLE 200, Laser Technik Berlin) is equipped with an Echelle grating, where the achieved spectral resolution is 15.9 to 31.8 pm. Before any measurement took place, the focus was adjusted to the jet axis and the spectrometer was calibrated with a spectral Hg lamp. The lenses were focused at 700 and 900 mm, respectively, and at these distances, the emission spectra were recorded. They were used to determine the molar volumetric vapor concentrations of W and La by analyzing the intensities of two neutral W I and La I emission lines at 429.4605 and 521.186 nm considering the corresponding energy levels and transition probabilities. These two lines were detectable at all studied plasma compositions as they are well isolated and not self-absorbing. In addition to the emission line data, the excitation temperatures at the different investigated plasma compositions were required. They were determined by Boltzmann plots [23] based on a set of neutral Ar I emission lines corresponding to the transition 5p-4s [22]. As mentioned above, LTE was assumed which is a necessary requirement to apply this method. Furthermore, the same temperatures can be implied for the Ar, La and W species.

2.5. Stoichiometry determination of LaWO coatings

Preliminary experiments were carried out using graphite as a substrate material aiming to adjust parameters versus LaWO coatings stoichiometry. By this, free-standing layers were obtained by annealing after spraying in air at 600°C to remove the substrates. Due to the relatively low temperature, it can be assumed that this step did not affect the La/W stoichiometry or the phases present in the coatings. The chemical composition of the coatings was determined using inductively coupled plasma-optical emission Spectrometry (ICP-OES, error ± 3%). The oxygen content was determined by means of He carrier gas hot extraction

including infrared (IR) absorption (LECO TCH-600, 0.5% relative standard deviation for O_2). Finally, the stoichiometry was calculated.

2.6. Phase characterization of LaWO coatings

X-ray diffraction analyses (XRD, D4 Endeavor-Bruker AXS with Cu-K_α radiation) were performed to determine the phase compositions of the fabricated LaWO coatings. Phases were identified using ICDD PDF2-Database (Release 2004), ICSD Database (Release 2017) and X'Pert Highscore Plus (by PANalytical). The reference patterns correspond to the cards ICSD 252211 ($La_{6.75}W_{1.25}O_{13.5}$), PDF No. 01-074-2430 ($La_2O_3$) and ICSD 247427 ($La_6W_2O_{15}$) for phase identification. For Rietveld analysis, the TOPAS V 4.2 software was used.

2.7. Phase evolution in LaWO coatings at high temperatures

High-temperature x-ray diffraction analysis (HT-XRD, Empyrean-PANalytical GmbH) was carried out using the environmental heating chamber (HTK1200N-Anton Paar GmbH) in order to assess the stability of the main phase and secondary phase evolution as function of the temperature. Measurements were carried out in air at atmospheric pressure. Scans were taken in the Bragg angle range from $2\theta = 20°$ to 80° in 0.026° steps with 20 min of data-collecting time at each temperature. The XRD data were collected at room temperature (before and after the heating cycle, later referred to as ground state 1 and 2, respectively), as well as at 900°C and 1000°C with heating rate of 5K/min. In addition, measurements of the original feedstock were carried out at low pressure (10^{-2} Pa, Ar atmosphere).

2.8. Microstructure and residual stress analysis of the PS-PVD sprayed LaWO coatings

Grain orientation, morphology and size distribution in LaWO layers were determined by means of electron backscattering diffraction (EBSD) measurements to elucidate the effect of

heat treatments on grain evolution of selected PS-PVD coatings. They were carried out using a SEM JSM-7000F by JEOL equipped with a camera "Hikari" and an "Octane Plus-A" detector for EDX (both by Ametek-EDAX). Areas of 200x75 μm were analyzed with a step size of 100 nm at 20 keV electron energy and probe current of approximately 30 nA. Data were processed and analyzed with OIM Data Collection V 7.3 and OIM Analysis V 8.0 software. Additionally, phase distribution, grain sizes, morphology and boundary structure were studied by means of kernel average misorientation (KAM) mappings. Furthermore, stress analysis of the coatings was performed based on the KAM mappings to elucidate the effect of deposition process and secondary phase formation. KAM analysis gives a qualitative measure of the stored strain energy in a sample.

3. Results and Discussion

3.1. Effect of the plasma spray parameters on cation evaporation

Table 3 summarizes the stoichiometries calculated from the ICP-OES chemical analyses. A comparison of the molar ratios of tungsten and lanthanum in the two coatings with the original feedstock reveals that for all coatings the La/W ratio increases from the initial value of 5.55. This fact can be associated with W evaporation during the spraying, which is supported also by earlier literature sources [11,12]. As it can be inferred from the table, coatings A/1 and B/1 exhibit higher La/W ratios than coating C/1. This is a clear indication that inhomogeneous evaporation of feedstock species takes place during plasma spraying and that it grows with increase in thermal treatment of the particles.

Table 3. **Molar ratios of tungsten and lanthanum from the chemical analysis by ICP-OES for the LaWO feedstock and functional layers deposited on graphite without addition of O_2.**

LaWO	**Molar ratio La/W**
Feedstock	5.55
Coating A/1	5.85
Coating B/1	5.89
Coating C/1	5.62

In order to verify the evaporation of cations during the spray process, an additional assessment of the plasma jet was conducted based on OES focusing on two distinct emission lines of neutral W I and La I. The results showed that at both plasma parameters used to fabricate coatings A/B and C (see Table 1), evaporation of La and W cations takes place. However, it is less intensive for parameter C, which is consistent to the finding that the thermal treatment of the feedstock is less than for parameters A/B. To conclude on the thermal history during flight, one measurement was performed for parameter C also at a shorter spray distance of 700 mm although no samples were sprayed at this position. As it can be inferred from Figure 2, the overall vapor concentrations are higher than at 900 mm which is expected because of the higher plasma temperatures. However, the gap between W and La is larger than at 900 mm. This is an indication that the inhomogeneity of evaporation during flight is significant as W evaporates preferably.

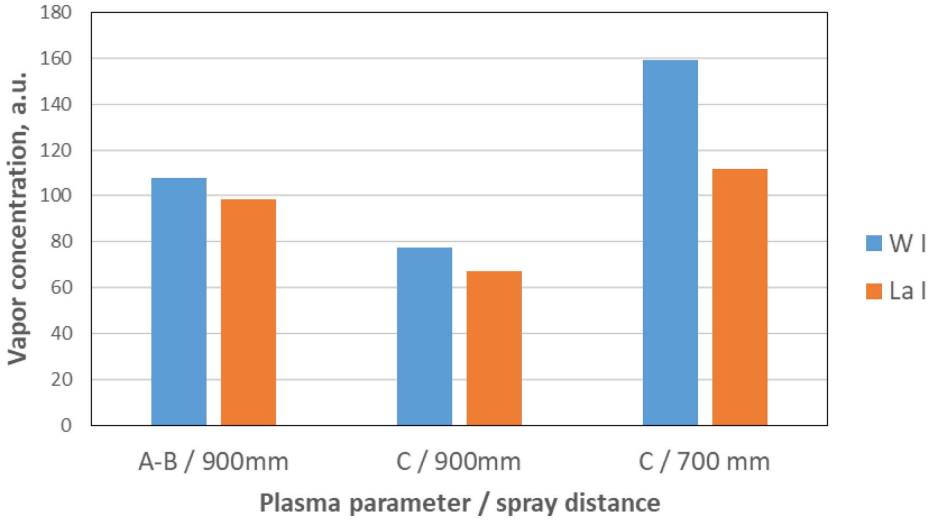

Figure 2. Vapor concentrations from OES for the plasma parameters A/B and C at spray distances of 900 mm and 700 mm, respectively; the units are proportional to the number of moles per unit volume.

Figure 3 presents the dependence of the vapor pressure on the temperature for different compounds. WO_3 evaporates first followed by La, La_2O_3 and finally W. Thus, the preferential evaporation of WO_3 is assumed to be the reason that the molar La/W ratio is affected during spraying leading to an excess of La in the deposits.

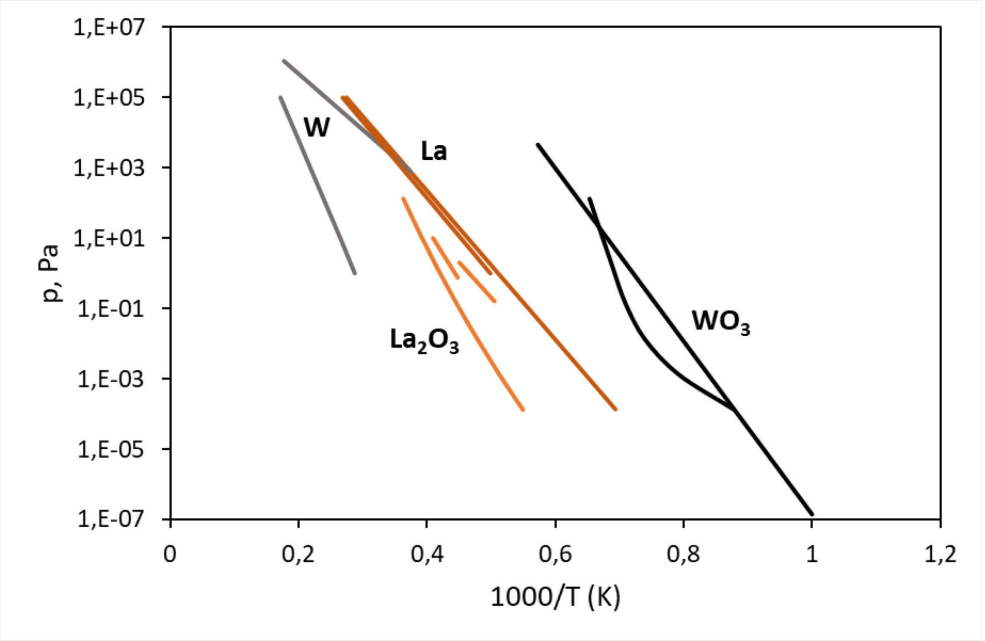

Figure 3: **Vapor pressures as function of the temperature for different compounds; data taken from Yaws (1995), Gmelin (1974), Samsonov (1986), Magrave (1967).**

3.2. Effect of the spray parameters on phase formation in LaWO coatings

Figure 4 presents the XRD patterns corresponding to as-sprayed samples A/1, B/1 and C/1. Additionally, the quantification of the phases obtained from the Rietveld refinement is summarized in Table 4.

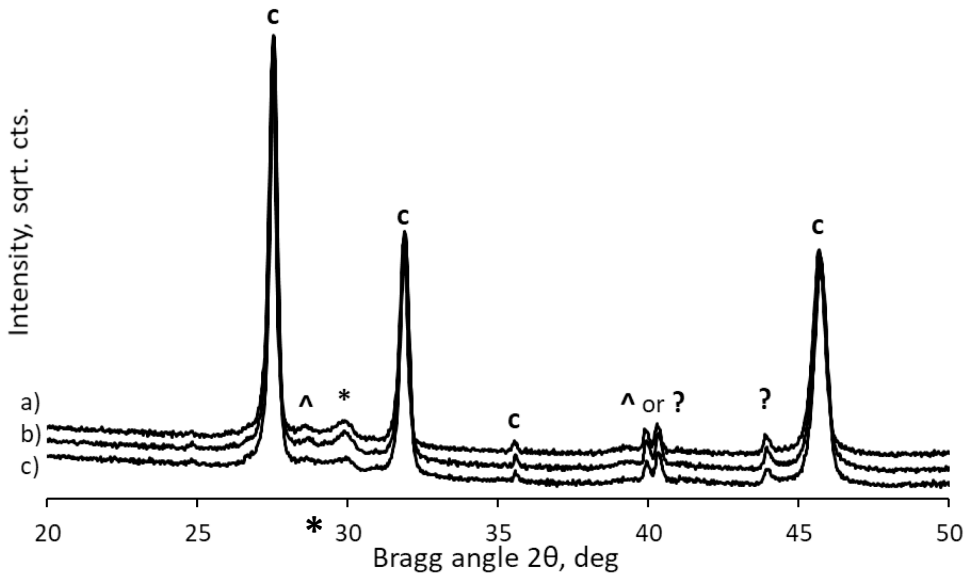

Figure 4. XRD pattern of plasma sprayed samples on graphite with different spraying distances/plasma conditions a) coating A/1, b) coating B/1, c) coating C/1; c: cubic LaWO, *: La_2O_3 (main peak at approx. 30°), ^: $La_6W_2O_{15}$ (main peak at 28°-29°), and ?: not absolutely certain.

Table 4. Phase composition of LaWO coatings sprayed on graphite; spraying was carried without addition of O_2 during the processing; the percentages denote fractions as determined from the Rietveld analysis.

Sample	**LaWO cubic (%)**	**$La_6W_2O_{15}$ (%)**	**La_2O_3 (%)**
Feedstock	100	-	-
Coating A/1	89	3	8
Coating B/1	93	2	5
Coating C/1	98	-	2

As it can be inferred from the obtained results, the coatings consist predominantly of the main cubic LaWO phase. However, the undesired secondary phases La_2O_3 and $La_6W_2O_{15}$ were also ascertained in more pronounced amounts for coatings A/1 and B/1. Furthermore, it can be observed that the quantity of the cubic phase increases when the spraying distance becomes smaller at the same plasma composition (coatings A/1 and B/1). That would mean that 900 mm distance (shorter thermal feedstock treatment) allows for better control over the resulting phase composition of the coating. Changing the plasma composition toward lower temperatures (coating C/1 versus coating B/1) at the same distance of 900 mm leads to further improvement of the phase composition (coating C/1 discloses 2% phase impurity compared to 7% for coating B/1).

In the work by Cadoret *et al.* [13], La-rich LaWO showed decomposition into co-existing La_2O_3 and $La_6W_2O_{15}$ phases at 10^{-6} mbar and 1000°C. Above, also a decreasing and even disappearance of the La_2O_3 phase was observed. This resembles the results of Shimura [1] and later by Seeger and Magraso [4,12] showing that the stability range of the cubic LaWO phase shifts to higher La/W ratios with increase in the processing temperature. Obviously, the LaWO solid solution at increased temperature (1500-1550°C) features the incorporation of more La_2O_3 without precipitating La_2O_3 secondary phase as it is the case at lower temperature (e.g., 1200-1300°C).

In contrast to the experimental conditions in the referenced works, in the PS-PVD process investigated here, the coatings were sprayed on substrates with surface temperatures of 800-900°C. Due to the very rapid cooling rates at particle impact, it is apparently possible to lock highly La-saturated compositions, which is in line with our observation of increased lattice parameter of the coatings (see section 3.5). Thus, the PS-PVD process is advantageous, also in view of the disproportional evaporation of W during flight, which shifts the stoichiometry to the La-rich domain. Evidently, the best condition is the parameter C as the temperatures are the lowest and the flight time is the shortest.

3.3. Effect of the support on the phase characteristics of the coatings

Typical cooling rates of the impacting feedstock particles are extremely high in the PS-PVD process and it has been shown in previous works [15,23-25] that phases existing at high temperatures were retained at room temperature. In addition, the effect of the supporting materials plays an important role due to different thermal conductivities. In this section, coatings C/1 and C/2 deposited on graphite and Crofer substrates, respectively, are compared. Figure 5 depicts the reference XRD pattern of the feedstock and for the two coatings. It is evident that the variation of the substrate material has a pronounced impact on the phase characteristics of material. The main peaks (222) and (004) are assigned with the main cubic phase, as denoted in the graph.

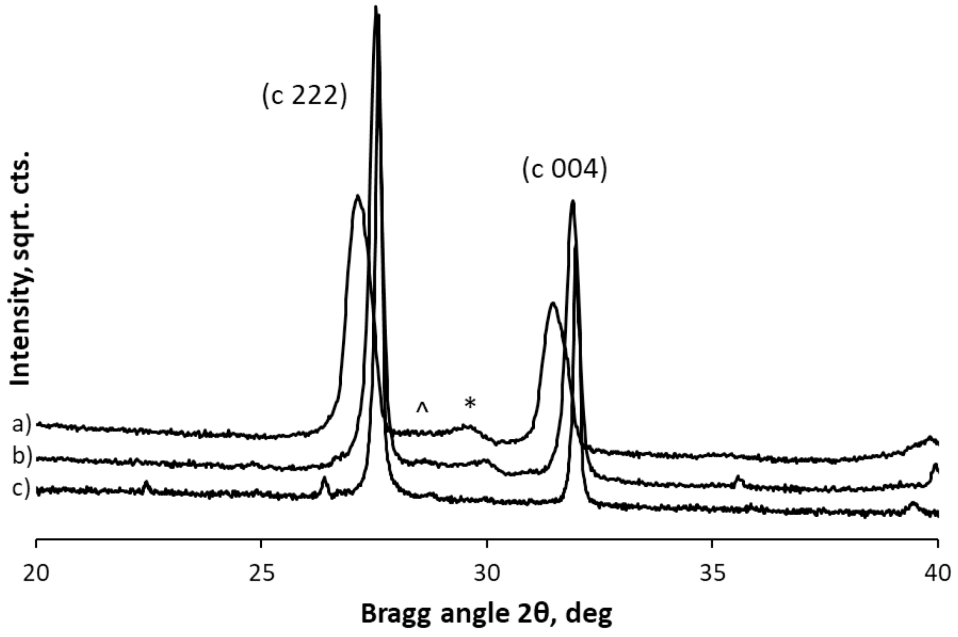

Figure 5: **Excerpts of the XRD patterns for coatings sprayed on a) Crofer (coating C/2), b) graphite (coating C/1) and c) feedstock; *:La_2O_3, ^:$La_6W_2O_{15}$.**

For the feedstock, these peaks are well defined and sharp. Comparing the main peaks recorded for the reference material and for the two coatings on graphite (C/1) and on Crofer (C/2), respectively, peak broadening and also shifts to smaller Bragg angles are noticeable.

The observed peak broadening effects reflect strains, different solid solution homogeneities and crystallite sizes. They will be discussed later. Apart from the broadening, slight peak shifts to the left, particularly for coating C/2, are visible. Coatings obtained on graphite and Crofer exhibited lattice constants equal to 11.225(1) Å and 11.247(1) Å, respectively, while that of the reference material was determined to be 11.180(1) Å. The observed increase in the lattice constant can be assigned to oxygen release from the material due to the reducing processing conditions. This could also be evidenced by the gray sample color, while samples sintered in air are typically white. Further peak shifts may be introduced by strain effects to different extents due to the thermal mismatch of coatings and substrates.

Coatings on graphite (C/1) experienced slower cooling rates than on Crofer (C/2) due to the different designs of the sample holder (see Sect. 2.3) leading to a smaller heat removal rate in the first case, although graphite reveals a higher thermal conductivity than Crofer. The XRD pattern for the graphite supported coating C/1 is hence more consistent with the reference pattern as slow cooling favors crystallite growth. Furthermore, the Crofer supported coating C/2 showed a slight peak attributed to the La_2O_3 precipitate, which, however, is slightly shifted from its 30° reference position.

3.4. Effect of O_2 addition during the PS-PVD processing on the phase formation

Secondary phase evolution and distribution as a function of the O_2 addition during the spray processing was studied by means of HT-XRD at 900°C and 1000°C in air. Figure 6 presents the HT-XRD patterns collected for Crofer supported coatings C/3 (sprayed without addition of O_2) and C/4 (sprayed with addition of 4 slpm O_2 to the process chamber atmosphere).

Figure 6 (top) shows the evolution (RT→1000°C→RT, in air) of the LaWO coating without addition of O_2 during the spraying. Ground state 1 (solid line at RT) shows a slight presence of secondary phases (low intensity $La_6W_2O_{15}$ peak). Ground state 2 (dotted line at RT) reveals a more pronounced quantity of the $La_6W_2O_{15}$ phase. At temperatures lower than 900°C, the $La_6W_2O_{15}$ peak remained unchanged (spectra not shown here) and its intensity increases at 1000°C. Since the La_2O_3 peak remained nearly unchanged, it is assumed that at 1000°C and above, La_2O_3 is segregated from the LaWO phase, while it is consumed at the same time by the formation of $La_6W_2O_{15}$.

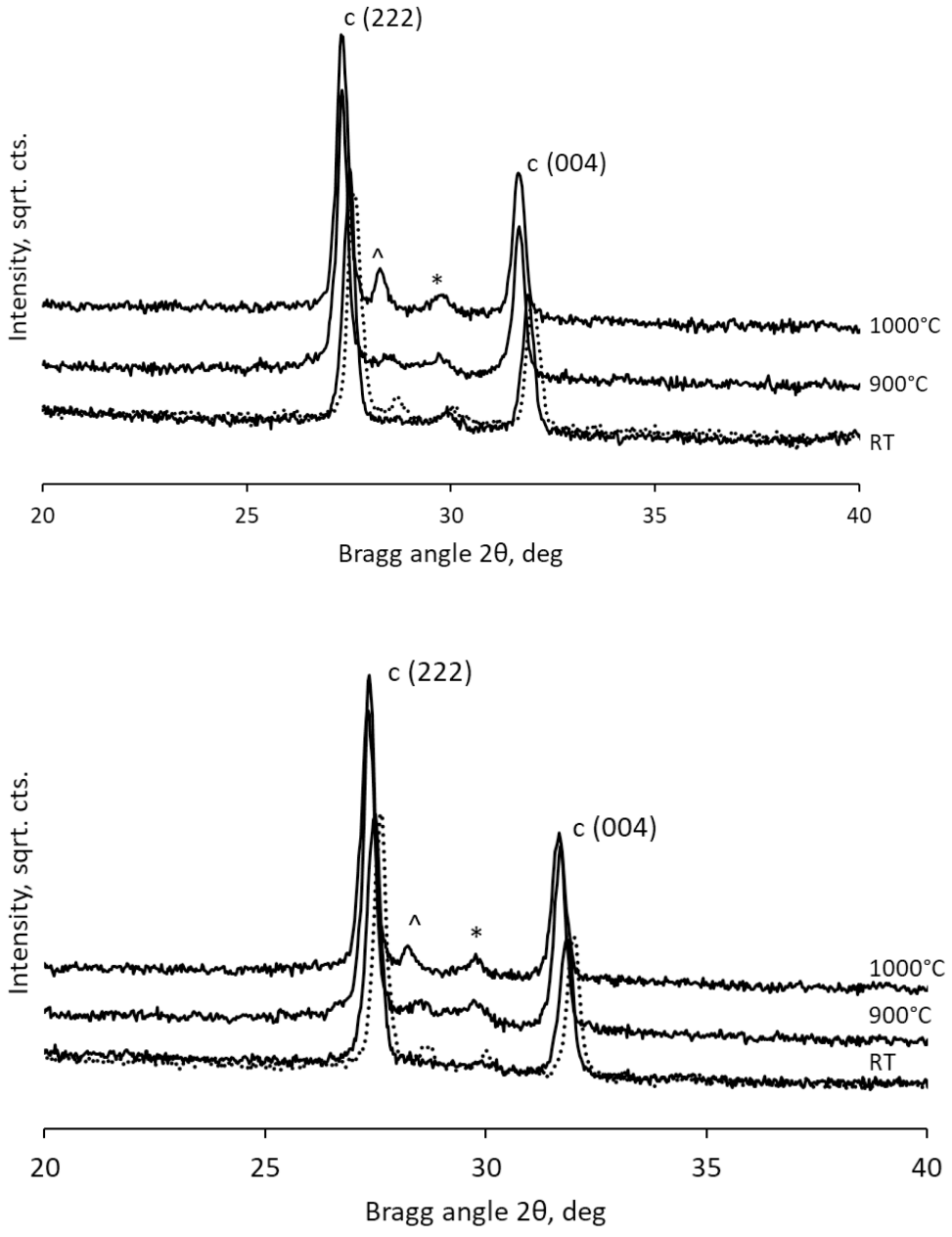

Figure 6. HT-XRD patterns collected in air for LaWO coatings C/3 sprayed without extra O_2 (top) and C/4 sprayed with 4 slpm O_2 (bottom); c:cubic phase, *: La_2O_3, ^: $La_6W_2O_{15}$ phases; XRD patterns at RT are given as reference measurements: solid line corresponds to ground state 1 before heating, while the dotted line corresponds to ground state 2 after the cooling.

Figure 6 (bottom) depicts the evolution (RT→1000°C→RT in air) of the LaWO coating sprayed with addition of O_2. As expected, no $La_6W_2O_{15}$ peak is present before the heat treatment, and the La_2O_3 is almost negligible (considering the measurement error and the limited resolution of the HT-XRD measurements). At 900°C and 1000°C these phases evolve but to a smaller extent compared to C/3. As a result, the XRD pattern of ground state 2 shows reduced secondary phase peaks.

Table 5 summarizes quantitatively the phase compositions at RT and 1000°C obtained from the Rietveld analysis of the HT-XRD patterns.

Table 5. **Phase compositions of coatings C/3 and C/4 on Crofer at RT and 1000°C according to the Rietveld analysis of the HT-XRD patterns (uncertainties ± 1%).**

O_2 supply during spray processing, slpm	**LaWO, cubic (%)**	**$La_6W_2O_{15}$ (%)**	**La_2O_3 (%)**
RT			
- (C/3)	95	-	5
4 (C/4)	98	-	2
1000ºC			
- (C/3)	94	4	2
4 (C/4)	97	2	1

As it can be inferred from these results, the addition of O_2 during the spray processing leads to an increased content of the main phase and diminished formation of secondary phases. Adding O_2 during spraying can be linked to stabilization of the cubic phase by filling oxygen vacancies as it can be inferred also from the lattice constants: 11.247(1) Å for C/3 versus 11.229 (1) Å for C/4. Furthermore, it is evident that the phase composition will be practically stable at membrane operating conditions at typical temperatures below 800-850°C.

3.5. Lattice constant as function of the processing parameters

Figure 7 gives a graphical representation of the lattice constant as a function of the processing conditions. As shown in the graph, the values for the PS-PVD coatings (C1-C4) are larger than those of the feedstock (FS, La/W 5.5) and Ref. [12] (La/W 5.5). This indicates a higher degree of lattice expansion for the PS-PVD processed coatings which might be associated with a higher oxygen vacancy concentration. This is also known from other plasma sprayed oxide ceramics [26]. High amounts of point defects benefit the conductivity properties of the obtained material and thereof deposited coatings. As indicated earlier [27], the oxygen deficiency plays an important role for the hydration and electrical properties of the proton conductors. Oxygen vacancy concentration and La/W ratio are in a defect-chemical correlation: one W^{6+} on a La^{3+} site will neutralize 1.5 oxygen vacancies ($W_{La}^{\cdots}$ acts as a donor). Therefore, structures rich in W, i.e., at lower La/W ratio, exhibit a compromised conductivity but are stable, while at higher La/W ratios, the material has an increased conductivity but with compromised stability (within certain tolerance range). In this context, the electrical conductivity of LaWO based materials in humid atmospheres was shown to increase with increasing the La/W ratio [12]. Such observations are in line with the H_2 permeation performance of the PS-PVD LaWO membrane reported earlier by our group [28] as the H_2 permeation is directly proportional to the ambipolar conductivity of the material. The H_2 permeation of a 60 µm thick LaWO gas separation membrane on Crofer was ca. 0.4 ml/min·cm^2 at 825°C, which is the highest value for LaWO supported assembly at application relevant temperatures reported so far [29]. This exceptional performance is comparable with that of newly developed dual phase cer-cer and cer-met membranes [30,31].

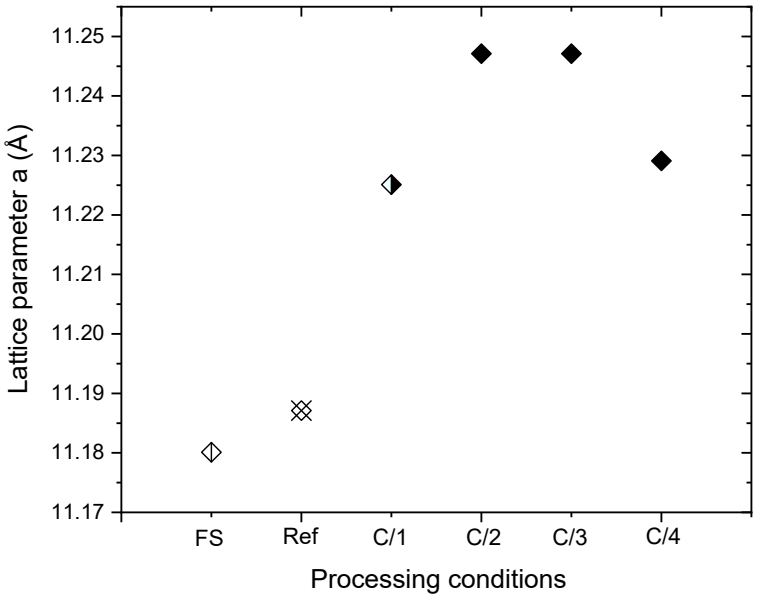

Figure 7. Lattice constant of the main LaWO cubic phase as function of the processing conditions. FS: feedstock; Ref: [12]; C/1: graphite supported coating; C/2-C/4: Crofer supported coatings.

It can be concluded that the reducing PS-PVD conditions generally affect the lattice parameters. As explained above, the cooling rate of the graphite substrates is lower than for the Crofer substrates due to the different sample dimensions and concepts of sample holders. If sprayed on graphite, this obviously results in less La in the LaWO phase, and moreover in less solution non-homogeneities and less strain effects (C/1 and C/2, respectively). Annealing in air has no particular effect compared to annealing under 10^{-2} Pa Ar (C/2 and C/3, respectively). However, the addition of O_2 to the process chamber atmosphere apparently changes the oxygen equilibrium and leads to a reduction in oxygen vacancies (C/3 and C/4, respectively).

3.6. Microstructure, morphology, strain effects and texture of the LaWO coatings

Figure 8 presents EBSD micrographs of LaWO coatings C/7 and C/8 both sprayed with O_2 addition and thereafter annealed under Ar (10^{-2} Pa) or air (atmospheric pressure), respectively, from which phase distributions could be ascertained.

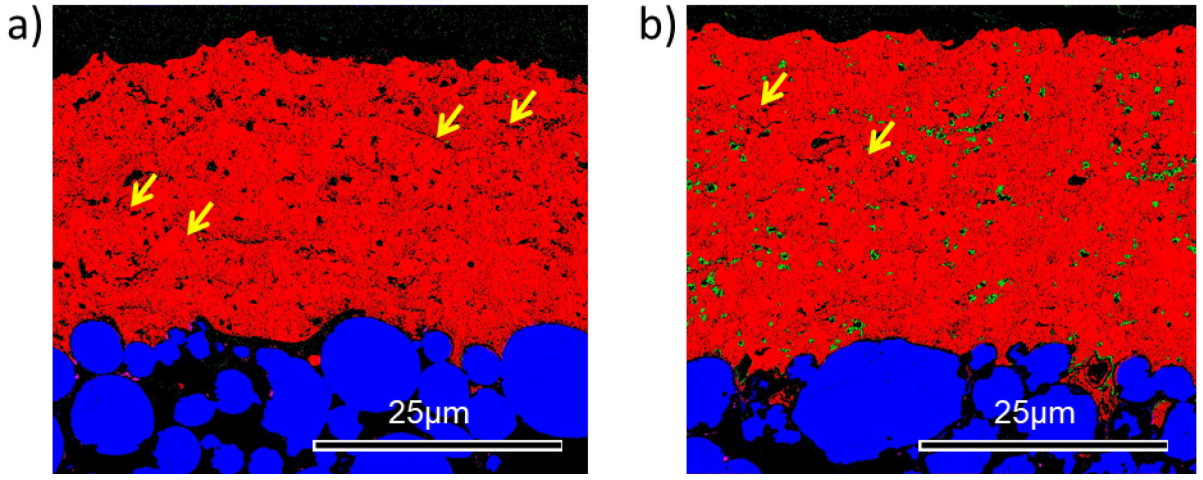

Figure 8. EBSD micrographs showing phase distributions of the main cubic LaWO phase (red) and the secondary phases La_2O_3 (pointed by yellow arrows) and $La_6W_2O_{15}$ (green) in a) sample C/6 coated with extra O_2 and annealed in Ar and b) in sample C/7 coated with extra O_2 and annealed in air; the coating contains mainly the cubic LaWO phase (red), while the secondary phases La_2O_3 (yellow) and $La_6W_2O_{15}$ (green) are in negligible amounts; $La_6W_2O_{15}$ is more likely to be found surrounding pores after contact with air.

After annealing in Ar or air, the content of the secondary phase La_2O_3 is very small as indicated by the arrows. After annealing in air, $La_6W_2O_{15}$ is observed. These results are in agreement with the observations made via the XRD and HT-XRD analyses. Interestingly, this phase as well as the La_2O_3 was found around pores or inside cracks, i.e., surfaces exposed to oxidation.

Stored strain energy was analyzed for these coatings sprayed with addition of oxygen. Figure 9 shows kernel average misorientation (KAM) mappings displaying a homogenous distribution of the stored energy. From Figure 9 a), it can be recognized that the light green areas are not associated with the La_2O_3 impurities. Figure 9 b) shows the same situation as the light green areas are not associated with secondary phases.

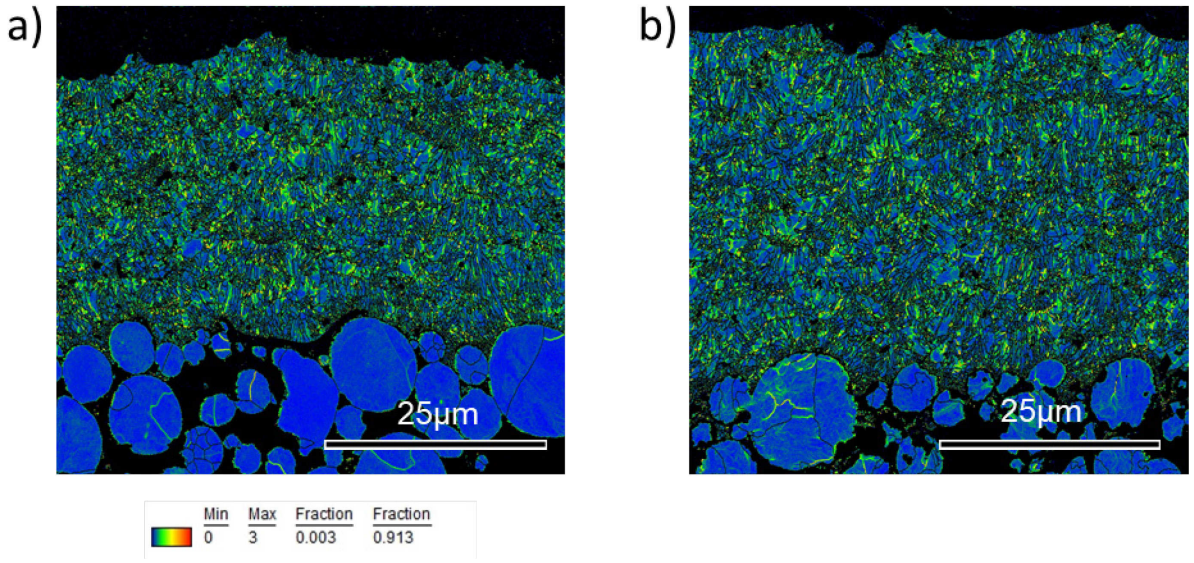

Figure 9. EBSD Kernel Average Misorientation mappings (KAM, 100 nm, 5°); stored strain energy in LaWO dense coatings; a) coating C/6; b) coating C/7; the higher level of misorientation, and therefore strain, is seen in the brighter green color.

The KAM analysis shows that the lattice deformation is basically concentrated around the sub-grain boundaries and not particularly around the secondary phases. This was observed for coatings C/6, in which the amount of secondary phase La_2O_3 is negligible, as well as for C/7 with $La_6W_2O_{15}$ impurities. This lets us conclude that there is no deleterious effect of the presence of secondary phases (low amounts) with respect to residual stresses accumulation and to the integrity of the coatings.

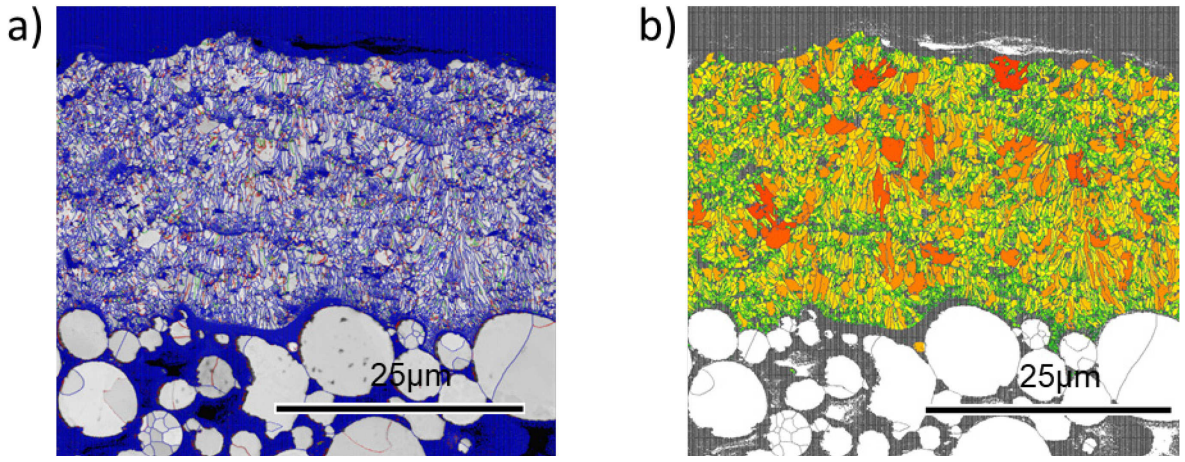

Figure 10. EBSD grain orientation, morphology and sizes for sample C/6; a) grain boundaries (blue: high-angle grain boundaries, green: low-angle grain boundaries, red: sub-grain boundaries); b) grain morphology and sizes (green: 0.2-0.8 µm, yellow: 0.8-1.6 µm, orange: 1.8-3.1 µm, red: 3.5-10 µm).

Figure 10 shows the morphology of the sample C/6 annealed in Ar. Analyzing the grain boundary distributions of the coating, it was found that high-angle grain boundaries form the majority with only a few low angle or sub-grain boundaries. The grain elongation is mainly perpendicular to the substrate, which is consistent with the thermal flux during solidification of the deposited splats. The few low-angle grain boundaries might be resulting from residual stresses introduced by quenching the individual particles from their molten state. Recrystallization during annealing is obviously not significant.

4. Conclusions

We carried out a systematic study of the LaWO ceramic layers formation on porous metallic substrates as a function of the PS-PVD processing parameters as plasma characteristics, support type and temperature, as well as addition of O_2 during the spraying. One advantage of the PS-PVD manufacturing route is that porous steel supports can be applied as they can

be coated directly without any interlayer. Moreover, no subsequent sintering at elevated temperatures is required. A set of processing conditions was established, leading to purely cubic LaWO layers with negligible secondary phase precipitations (≤ 2%), excellent He gas tightness in the range of 10^{-3}-10^{-4} mbar·l/s·cm^2 (98-99% coating density) and earlier demonstrated unprecedented H_2 permeation performance of ca. 0.4 ml/min·cm^2 at 825°C and 60 µm coating thickness [28]. The phase formation and evolution was strongly affected by the cation and oxygen stoichiometries, being dependent on processing parameters and additionally on the reducing atmospheres and the very fast cooling rates. By means of the PS-PVD technique, coatings consisting predominantly of single cubic LaWO phase could be obtained at lower temperatures (800-900°C) than conventionally applied (1450-1550°C), and also for much shorter times. Furthermore, it was found that the colder spraying conditions lead to milder W evaporation which kept the La/W ratio within the single phase domain without formation of significant phase impurities. On the other side, the hotter plasma spray conditions allowed for obtaining coatings with La/W ratio as high as 5.8-5.9 but with more pronounced amounts of secondary phase inclusions. The phase evolution could be affected by the addition of O_2 to the process chamber, which then is incorporated into the crystal lattice as evidenced by the lattice constant decrease, thus stabilizing the main LaWO phase. In any case, even if some amounts of the secondary phases were present (as long as they are minimal), they would not significantly affect the thermo-mechanical stability of the LaWO coatings at application relevant conditions. The rapid cooling of the feedstock at particle impact on the substrate led to formation of highly La-saturated compositions. Increased La contents relate with higher oxygen deficiency in the coatings, which indeed was confirmed by the significantly higher lattice parameter of the PS-PVD processed layers compared to the conventionally produced samples. Such lattice expansion plays a beneficial role for the hydration properties of the deposited functional layers. These observations are in line with the high H_2 permeation value obtained for the LaWO layer as reported earlier. Finally, the deposited layers exhibited fine grain microstructure, low levels of residual thermo-mechanical stresses and appreciable phase stability at application relevant temperatures.

Acknowledgements

The authors gratefully acknowledge Mr. Ralf Laufs for his help with the use of the PS-PVD facility. D.M. thanks for funding from the European Community's Seventh Framework Programme, FP7/2007-2013, under Grant Agreement No. 241309 (DEMOYS Project). M.I. thanks BMBF, Germany, for the financial support under grant 03SF0537A (ProtOMem project).

References

[1] H. Shimura, T. Fujimoto, S. Iwahara, Proton conduction in non-perovskite-type oxides at elevated temperatures, Solid State Ionics, 143 (2001) 117–123.

[2] R. Haugsrud, Defects and transport properties in Ln_6WO_{12} (Ln=La, Nd, Gd, Er), Solid State Ionics, 178 (2007) 555–560.

[3] C. Haugsrud, R. Kjoelseth, Effects of protons and acceptor substitution on the electrical conductivity of La_6WO_{12}, J. Phys. Chem. Solids. 69 (2008) 1758–1765.

[4] J. Seeger, M.E. Ivanova, W.A. Meulenberg, D. Sebold, D. Stöver, G. Scherb, S. Schumacher, S. Escolástico, C. Solis, J.M. Serra, Synthesis and Charaterization of Nonsubstituted and Substituted Proton-Conducting $La_{6-x}WO_{12-y}$, Inorg. Chem. 52 (2013) 10375–10386.

[5] D. van Holt, E. Forster, M. E. Ivanova, W.A. Meulenberg, M. Müller, S. Baumann, R. Vaßen, Ceramic materials for H_2 transport membranes applicable for gas separation under coal-gasification-related conditions, J. Eur. Cer. Soc., 34 (2014) 2381.

[6] E. Forster, D. van Holt, M. E. Ivanova, S. Baumann, W.A. Meulenberg, M. Müller, Stability of ceramic materials for H_2 transport membranes in gasification environment under the influence of gas contaminants, J. Eur. Cer. Soc., 36 (2016) 3457

[7] J.L. Vineet Gupta, Ceramic Proton Conductors, in: M.M. Anthony Sammels (Ed.), Nonporous Inorg. Membr., Wiley-VCH Verlag GmbH, Weinheim, 2006: pp. 49–76.

[8] M. Marrony, H. Matsumoto, N. Fukatsu, M. Stoukides, Applications of Proton Ceramic Cells: A Way to Market, Proton Conducting Ceramics: From Fundamentals to Applied Research, M. Marrony (Edt.), Pan Stanford Publishing Pte. Ltd., ISBN 978-981-4613-84-2 (2016) 291-405.

[9] G. Kojo, X. Wei, Y. Matsuzaki, H. Matsuo, K. Hellgardt, J. Otomo, Fabrication and electrochemical performance of anode-supported solid oxide fuel cells based on proton-conducting lanthanum tungstate thin electrolyte, Solid State Ionics 337 (2019) 132-139.

[10] W. Deibert, M.E. Ivanova, S. Baumann, O. Guillon, W.A. Meulenberg, Ion-Conducting Ceramic Membrane Reactors for High-Temperature Applications, J. Memb. Sci. (2017) 543, p 79-97, https://doi.org/10.1016/j.memsci.2017.08.016.

[11] A. Fantin, T. Scherb, J. Seeger, G. Schumacher, U. Gerhards, M. E. Ivanova, W. A. Meulenberg, R. Dittmeyer, J. Banhart, Crystal structure of Re-substituted lanthanum tungstate $La_{5.4}W_{1-y}Re_yO_{12-\delta}$ ($0 \leq y \leq 0.2$) studied by neutron diffraction, J. Appl. Cryst., 49 (2016) 1544

[12] A. Magraso, C. Frontera, D. Marrero-Lopez, P. Nunez, New crystal structure and characterization of lanthanum tungstate "La_6WO_{12}" prepared by freeze-drying synthesis, Dalt. Trans. (2009) 10273–10283.

[13] K. Cadoret, F. Millot, J. de Cachard, L. Martinez, L. Hennet, A. Douy, M. Licheron, Chemical behaviour of Lanthanides-Tungsten composite materials used in thermo-emissive cathodes, Eds. G. Kneringer, P. Rödhammer, H. Wildner, Proc. Plansee Semin. (2001) Vol. 1, p 669–683.

[14] M.E. Ivanova, J. Seeger, J.M. Serra, C. Solis, W.A. Meulenberg, W. Fischer, S. Roitsch, H.P. Buchkremer, Influence of the $La_6W_2O_{15}$ phase on the properties and integrity of $La_{6-x}WO_{12-d}$ based membranes, Chem. Mater. Res. 2 (2012) 56–82.

[15] M.O. Jarligo, G. Mauer, M. Bram, S. Baumann, R. Vaßen, Plasma Spray Physical Vapor Deposition of $La_{1-x}Sr_xCo_yFe_{1-y}O_{3-\delta}$ thin-film oxygen transport membrane on porous metallic supports, J. Therm. Spray Technol. 23 (2014) 213–219.

[16] D. Marcano, G. Mauer, Y.J. Sohn, R. Vaßen, J. Garcia-Fayos, J.M. Serra, Controlling the stress state of $La_{1-x}Sr_xCo_yFe_{1-y}O_{3-\delta}$ oxygen transport membranes on porous metallic supports deposited by plasma spray – physical vapor process, J. Membr. Sci. 503 (2016) 1–7. https://doi.org/10.1016/j.memsci.2015.12.029.

[17] D. Marcano, G. Mauer, R. Vaßen, A. Weber, Manufacturing of high performance solid oxide fuel cells (SOFCs) with atmospheric plasma spraying (APS) and plasma spray-physical vapor deposition (PS-PVD), Surf. Coatings Technol. 318 (2017) 170–177.

[18] W. Deibert, M.E. Ivanova, W.A. Meulenberg, R. Vaßen, O. Guillon, Preparation and sintering behaviour of $La_{5.4}WO_{12-d}$ asymmetric membranes with optimised microstructure for hydrogen separation, J. Membr. Sci., 492 (2015), p 439.

[19] W. Deibert, V. Stournari, M. E. Ivanova, S. Escolástico, J. M. Serra, J. Malzbender, T. Beck, W.A. Meulenberg, L. Singheiser, O. Guillon, Effect of microstructure on electrical and mechanical properties of $La_{5.4}WO_{12-\delta}$ proton conductors, J. Eur. Cer. Soc. 38 (2018) 3527.

[20] M. Bram, R. Kauert, H. P. Buchkremer, D. Stöver, Porous Materials Porous Metal Sheets Made By Tape Casting Of Metal Powders, EPMA, Proc. of Euro-PM 2003, 20–22 October 2003, Valencia, Spain 2003, 353–359.

[21] G. Mauer, Plasma Characteristics and Plasma-Feedstock Interaction Under PS-PVD Process Conditions, Plasma Chem. Plasma Proc. 34, 2014, No. 5, p 1171-1186. https://doi.org/10.1007/s11090-014-9563-z

[22] J.A. Aguilera, C. Aragon, Characterization of a laser-induced plasma by spatially resolved spectroscopy of neutral atom and ion emissions. Comparison of local and spatially integrated measurements, Spectrochim. Acta, Part B, 59 (2004) 1861–1876.

[23] G. Mauer, N. Schlegel, A. Guinard, R. Vaßen, O. Guillon, Effects of feedstock decomposition and evaporation on the composition of suspension plasma-sprayed coatings, J. Therm. Spray Technol. 24 (2015) 1187–1194.

[24] D. Marcano, G. Mauer, Y.J. Sohn, R. Vaßen, J. Garcia-Fayos, J.M., Serra, The role of oxygen partial pressure in controlling the phase composition of $La_{1-x}Sr_xCo_yFe_{1-y}O_{3-\delta}$ oxygen transport membranes manufactured by means of Plasma Spray-Physical Vapor Deposition, J. Therm. Spray Technol. 25 (2016) No. 4, p 631-638. https://doi.org/10.1007/s11666-016-0383-y

[25] G. Mauer, M.O. Jarligo, D.E. Mack, R. Vaßen, Plasma-sprayed thermal barrier coatings: new materials, processing issues, and Solutions, J. Therm. Spray Technol. 22 (2013) 646–658. https://doi.org/10.1007/s11666-013-9889-8.

[26] G. Mauer, N. Schlegel, A. Guignard, M.O. Jarligo, S. Rezanka, A. Hospach, R. Vaßen, Plasma Spraying of Ceramics with Particular Difficulties in Processing, J. Therm. Spray Technol. 24, 2015, No. 1-2, p. 30-37. doi: 10.1007/s11666-014-0149-3

[27] K.-D. Kreuer, Proton-conducting oxides, Ann. Rev. Mater. Res. 33 (2003) 333–359.

[28] M.E. Ivanova, W. Deibert, D. Marcano, S. Escolástico, G. Mauer, W.A. Meulenberg, M. Bram, J.M. Serra, R. Vaßen, O. Guillon, Lanthanum tungstate membranes for H_2 extraction and CO_2 utilization: fabrication strategies based on sequential tape casting and plasma-spray physical vapor deposition, Sep. Purif. Technol. 219 (2019) 100–112.

[29] V. Gil, J. Gurauskis, C. Kjølseth, K. Wiik, M.A. Einarsrud, Hydrogen permeation in asymmetric $La_{28-x}W_{4+x}O_{54+3x/2}$ membranes, Int. J. Hydrogen Energy 38 (2013) 3087–3091.

[30] M.E. Ivanova, S. Escolástico, M. Balaguer, J. Palisaitis, Y. J. Sohn, W.A. Meulenberg, O. Guillon, J. Mayer, J.M. Serra, Hydrogen separation through tailored dual phase membranes with nominal composition $BaCe_{0.8}Eu_{0.2}O_{3-\delta}$:$Ce_{0.8}Y_{0.2}O_{2-\delta}$ at intermediate temperatures, Scientific Reports, 6 (2016) 34773.

[31] D. Montaleone, E. Mercadelli, S. Escolástico, A. Gondolini, J.M. Serra, A. Sanson, All-ceramic asymmetric membranes with superior hydrogen permeation, J. Mater., Chem. A 6 (2018) 15718–15727.